

This is an Open Access document downloaded from ORCA, Cardiff University's institutional repository: <https://orca.cardiff.ac.uk/id/eprint/91125/>

This is the author's version of a work that was submitted to / accepted for publication.

Citation for final published version:

Compagnoni, Matteo, Kondrat, Simon A., Chan-Thaw, Carine E., Morgan, David John , Wang, Di, Prati, Laura, Villa, Alberto, Dimitratos, Nikolaos and Rossetti, Ilenia 2016. Spectroscopic investigation of Titania-supported gold nanoparticles prepared by a modified deposition/precipitation method for the oxidation of CO. *ChemCatChem* 8 (12) , pp. 2136-2145. 10.1002/cctc.201600072

Publishers page: <http://dx.doi.org/10.1002/cctc.201600072>

Please note:

Changes made as a result of publishing processes such as copy-editing, formatting and page numbers may not be reflected in this version. For the definitive version of this publication, please refer to the published source. You are advised to consult the publisher's version if you wish to cite this paper.

This version is being made available in accordance with publisher policies. See <http://orca.cf.ac.uk/policies.html> for usage policies. Copyright and moral rights for publications made available in ORCA are retained by the copyright holders.



# Spectroscopic Investigation of Titania-Supported Gold Nanoparticles Prepared by a Modified Deposition/Precipitation Method for the Oxidation of CO

Matteo Compagnoni,<sup>\*[a]</sup> Simon A. Kondrat,<sup>[b]</sup> Carine E. Chan-Thaw,<sup>[a]</sup> David J. Morgan,<sup>[b]</sup> Di Wang,<sup>[c]</sup> Laura Prati,<sup>[a]</sup> Alberto Villa,<sup>[a]</sup> Nikolaos Dimitratos,<sup>[b]</sup> and Ilenia Rossetti<sup>\*[a]</sup>

The spectroscopic characterization of a material is a fundamental tool for understanding the structure–activity correlation for catalytic purposes. Regarding supported nanoparticles, this perspective has acquired more relevance in recent years and several techniques have been employed. In this work diffuse reflectance infrared Fourier transform spectroscopy (DRIFTS), coupled with CO adsorption, was used to investigate a modified deposition/precipitation method (DP-UC) for the preparation of supported gold nanoparticles with very low metal loading (0.1–0.5 wt%). This promising synthetic route involves the

use of urea as basic agent and NaBH<sub>4</sub> as chemical reductant in contrast to the traditional high-temperature reduction step. The systematic IR spectroscopic study of the Au loading was combined with CO oxidation catalytic tests. The evaluation of the results was also supported by several other techniques, such as X-ray photoelectron spectroscopy, N<sub>2</sub> physisorption, and transmission electron microscopy. Particular attention was given to the evaluation of the gold electronic state, surface dispersion, particle size, and the corresponding structure–activity relationship.

## Introduction

Infrared absorption spectroscopy is considered one of the most promising methods to study catalyst surfaces. A multitude of different applications and experimental techniques are available,<sup>[1]</sup> such as transmission (TIR), attenuated total reflection (ATR), reflection–absorption (RAIRS) and diffuse reflectance (DRIFTS) modes. In this work, the latter technique was used, which allows us to analyze fragile solids, which are not amenable to manipulation, to produce self-standing samples with high intensity bands.<sup>[1]</sup> However, variations of scattering coefficients with cell geometry and sample loading remain the key parameters to consider. The use of this technique to investigate the adsorption of several probe molecules permits the

features of this method to be further extended.<sup>[2]</sup> Surface characterization with various NO<sub>x</sub> compounds was studied in depth by Hadjiivanov and co-workers,<sup>[3,4]</sup> and several basic probes are now widely used for the determination of surface acidity.<sup>[5,6]</sup> One of the most studied probes for metal nanoparticles is CO, which provides useful information about the metal surface exposure and the nature of metal sites.<sup>[5,7–9]</sup> Moreover CO is an important reactant in several industrial processes such as the production of methanol,<sup>[10]</sup> the Monsanto process, and in many cases it is an undesirable pollutant or poison.<sup>[11]</sup> The ability of this molecule to adsorb on nanoparticles is well known, especially in the case of Au, occurring through the formation of different surface carbonyls depending on the charge of the gold site, Au–support interaction, and particle size. This feature allows the discrimination of cationic, metallic, and anionic sites because of a direct correlation with CO absorption frequencies.<sup>[12]</sup>

Supported gold nanoparticles (AuNPs) have broad applications in many heterogeneous catalytic processes.<sup>[13,14]</sup> Several parameters influence the catalytic performance of AuNPs such as the particle size, the oxidation state, the nature of the support, the synthetic method, and the activation procedure for controlling the final morphology.<sup>[15]</sup> CO oxidation is one of the most studied processes<sup>[16,17]</sup> and allows the design of catalysts especially by considering Au particle size<sup>[18]</sup> and oxidation state. Indeed, it is well known that gold exhibits remarkable activity for CO oxidation when Au is highly dispersed on the support, such as TiO<sub>2</sub> and Fe<sub>2</sub>O<sub>3</sub>.<sup>[19,20]</sup> Moreover, this reaction is also important for other significant processes such as the water–gas shift step (WGS) in the H<sub>2</sub> purification sequence.<sup>[21,22]</sup> The oxidation state of Au during CO oxidation is a crucial but con-

[a] Dr. M. Compagnoni, Dr. C. E. Chan-Thaw, Prof. L. Prati, Dr. A. Villa, Prof. I. Rossetti  
Dip. Chimica  
Università degli Studi di Milano  
INSTM Unit Milano-Università and CNR-ISTM  
via C. Golgi, 19, I-20133 Milano (Italy)  
Fax: (+39)02-50314300  
E-mail: [matteo.compagnoni@unimi.it](mailto:matteo.compagnoni@unimi.it)  
[ilenia.rossetti@unimi.it](mailto:ilenia.rossetti@unimi.it)

[b] Dr. S. A. Kondrat, Dr. D. J. Morgan, Dr. N. Dimitratos  
Cardiff Catalysis Institute, School of Chemistry  
Cardiff University  
Main Building, Park Place, Cardiff, CF103AT (UK)

[c] Dr. D. Wang  
Institute of Nanotechnology  
Karlsruhe Institute of Technology  
Hermann-von-Helmholtz-Platz 1  
76344 Eggenstein-Leopoldshafen (Germany)

Supporting Information and the ORCID identification number(s) for the author(s) of this article can be found under <http://dx.doi.org/10.1002/cctc.201600072>.

troversial topic, largely debated in the literature.<sup>[12]</sup> Several works reported higher activity of oxidized gold than of metallic gold.<sup>[19,23]</sup> However, the adsorption of CO on Au<sup>n+</sup> is strongly inhibited by the presence of H<sub>2</sub>O, so metallic states are needed for the adsorption of CO and, hence, for the whole oxidation process.<sup>[24,25]</sup> On the other hand, different studies pointed out the important contribution of negatively charged Au.<sup>[26–28]</sup>

The preparation method is closely related to the dispersion, size, and electronic state of AuNPs, which in turn affects catalytic activity.<sup>[29]</sup> The deposition/precipitation (DP) method for the formation of highly dispersed gold nanoparticles on several oxidic supports is one of the most successful methods reported in the literature.<sup>[13,30–33]</sup> Urea (CO(NH<sub>2</sub>)<sub>2</sub>) is considered one of the most common basic agents for the DP method,<sup>[34,35]</sup> widely used also in other preparation procedures such as the co-precipitation synthesis.<sup>[36]</sup> Regarding the final reduction step, the use of sodium borohydride (NaBH<sub>4</sub>) as chemical reductant is a promising method at room temperature to obtain metallic gold nanoparticles with very narrow size distribution.<sup>[37]</sup> Its potential has also been proved for other metals, such as Pd,<sup>[38]</sup> Pt, and Sn.<sup>[39]</sup> However, the combination of these two steps is still relatively unexplored in the literature, especially for low metal loadings. Recently, Kumar and co-workers applied this synthetic route for the preparation of 1–4 wt% Au/TiO<sub>2</sub> samples for the oxidation of benzyl alcohol in the gas phase, with great success.<sup>[40]</sup> Therefore, the aim of the present work is to investigate several samples prepared by a new modified DP method with urea and chemical reduction (DP-UC), characterized by very low Au loading (0.1, 0.2, 0.5 wt%). Degussa P25 TiO<sub>2</sub> was chosen as a commercial support to eliminate any complications related to the support synthesis. In situ CO-DRIFT spectroscopy was used to identify and characterize the surface metal sites of the catalysts synthesized by the DP-UC method. The vibrational frequency of the C–O stretching is very sensitive to the strength and mode of bonding, but mainly it is related to the electronic state of the metal. In particular, the higher the frequency is (from 1900 to 2200 cm<sup>-1</sup>), the higher the charge of the metal site (from M<sup>n-</sup> to M<sup>n+</sup>).<sup>[7]</sup> Comparison of the band's position with other published reports leads us to emphasize that CO absorption frequencies are influenced by: (i) the partial pressure of CO in the gas flow,<sup>[29,41,42]</sup> (ii) the presence of other molecules such as H<sub>2</sub>O, O<sub>2</sub>, or H<sub>2</sub>,<sup>[25,43]</sup> and, mainly, (iii) by the adsorption temperature.<sup>[44]</sup> Therefore, the band's attribution was carried out by considering these key points, which is not always followed in the literature. Complementary techniques were used to shed light on the dispersion and local charge of the AuNPs, such as high-resolution (HR)TEM, STEM, and X-ray photoelectron spectroscopy (XPS). CO oxidation activity tests were carried out to better elucidate the nature of the particles and the catalytic performance was directly correlated to the exposure and electronic state of Au sites.

## Experimental Section

### Preparation of Au/TiO<sub>2</sub>

Gold nanoparticles were prepared by a modified deposition/precipitation method using urea and a chemical reductant (DP-UC). TiO<sub>2</sub> (1 g, Degussa P25, 50 m<sup>2</sup> g<sup>-1</sup>) was dispersed in distilled water (100 mL) with urea (5 g, Aldrich, >99%). NaAuCl<sub>4</sub>·2H<sub>2</sub>O solution (Aldrich, 99.99%) was added to the support and left under vigorous stirring for 4 h at 353 K. The catalyst was filtered and washed several times with water. The material was then suspended in distilled water and a freshly prepared solution of NaBH<sub>4</sub> (0.1 M, Fluka, >96%) was added (NaBH<sub>4</sub>/Au = 4 mol/mol) under vigorous stirring at room temperature. The sample was filtered, washed, and dried at 373 K for 4 h. The actual Au loading was checked by atomic absorption spectroscopic (AAS) analysis of the filtrate, with a Perkin-Elmer 3100 instrument. As expected using this method,<sup>[45]</sup> all the gold present in the solution was deposited on the support. Au/TiO<sub>2</sub> catalysts with the following compositions were prepared: 0.1, 0.2, 0.5 wt% Au/TiO<sub>2</sub>. Bare P25 was used as a reference.

### Characterization

DRIFTS studies were carried out with a Bruker Tensor 27 spectrometer fitted with a HgCdTe (MCT) detector, a Harrick Praying Mantis HVC-DRP-4 cell equipped with two ZnSe windows, and operated with OPUS software. The DRIFTS cell included gas inlet and outlet ports as well as capabilities for heating and cooling. The required gas flow, 40 cm<sup>3</sup> min<sup>-1</sup> of a 5% CO/N<sub>2</sub> gas mixture, was controlled by mass-flow controllers. The data are reported in the form of absorbance. Each spectrum represents an average of 64 scans collected with a spectral resolution of 2 cm<sup>-1</sup>. The ZnSe windows used cut off the spectrum below 650 cm<sup>-1</sup>; therefore, this region was not included in the discussion. In the reported spectra, a positive increase of peak intensity indicates an increase of population of that species, whereas a negative deflection shows loss of moieties associated with that particular mode. All samples were ground before the analysis. Background subtraction and normalization of the spectra were performed by subtracting spectra recorded under N<sub>2</sub> flow after heating the sample at 393 K for 30 min, to eliminate physisorbed and chemisorbed moisture. The gas-phase CO signal was removed by subtracting a spectrum obtained on pure KBr in a CO-containing atmosphere under the same analysis conditions.

Specific surface area and pore size distribution were evaluated through the collection of N<sub>2</sub> adsorption-desorption isotherms at 77 K on a Micromeritics ASAP 2020 instrument. Surface area was calculated on the basis of the Brunauer-Emmet-Teller equation (BET), whereas the pore size distribution was determined by the Barrett-Joyner-Halenda (BJH) method, applied to the N<sub>2</sub> desorption branch of the isotherm. Prior to the analysis, the samples were outgassed at 573 K for 24 h.

X-ray photoelectron spectroscopy (XPS) was performed by using a Kratos Axis Ultra-DLD photoelectron spectrometer that employed a monochromatic Al<sub>Kα</sub> X-ray source operating at 144 W power. High-resolution and survey scans were performed at pass energies of 40 and 160 eV, respectively. Spectra were calibrated to the C 1s signal at 284.8 eV, and quantified by using CasaXPS and modified Wagner sensitivity factors supplied by the manufacturer.

The specimens for transmission electron microscopy (TEM) were prepared by dispersing the catalyst powder on TEM grids coated with holey carbon film. They were examined by means of a FEI Titan 80–300 electron microscope equipped with CEOS image

spherical aberration corrector, Fischione model 3000 high-angle annular dark field (HAADF) scanning transmission electron microscopy (STEM) detector.

### Catalytic evaluation: CO oxidation

Catalytic activity for CO oxidation was investigated by using a fixed-bed U-shape glass reactor with 3 mm internal diameter placed in a thermostatically controlled oil bath. Reactive flow (5000 ppm CO in synthetic air) was fed to the reactor through mass flow controllers and 50 mg of catalyst was used to obtain a gas hourly space velocity (GHSV) of 4000 h<sup>-1</sup>. Analysis of the oxidation products was performed by using an online gas chromatograph equipped with a carbosieve column (3 m×35 mm) and a thermal conductivity detector. Before the test, all samples were dried in an oven overnight at 353 K. Conversion data were calculated relative to the CO<sub>2</sub> production and the detector was calibrated by using standard gas mixtures. Catalyst productivities are reported as turnover frequencies (TOFs) by considering the number of surface exposed atoms. Calculations of this parameter were performed by assuming that all the nanoparticles had cubic octahedral morphology with cubic close-packed structure in this size range by using the model of full-shell nanoparticles.<sup>[46]</sup>

$$\text{TOF-B} = \frac{\text{mol CO}}{\text{mol Au} \times \text{h}} \quad (1)$$

$$\text{TOF-N}_s = \frac{\text{TOF-B}}{A} \quad (2)$$

$$A = \frac{N_s}{N_t} \quad (3)$$

Where TOF-B is the TOF based on bulk Au using the weight measured by AAS, TOF-N<sub>s</sub> is based on the Au surface exposed atoms, A is the fraction of Au atoms lying at the surface,<sup>[47]</sup> N<sub>s</sub> is the number of Au surface atoms, and N<sub>t</sub> is the total number of Au atoms.

## Results and Discussion

### DRIFTS study of CO adsorption on the fresh Au/TiO<sub>2</sub> samples

For all the Au/TiO<sub>2</sub> samples analyzed, the presence of CO gave rise to one or two IR bands in the C–O carbonyl spectral region (1950–2150 cm<sup>-1</sup>). The IR band's assignment are presented in Table 1. The highest frequency band (2106 cm<sup>-1</sup>) was attributed to linearly adsorbed CO on metallic gold, in agreement with the literature.<sup>[32,41,44,48–50]</sup> Another broad and asymmetric band was detected at lower frequencies (Figure 1a). The maximum was located at 2072 cm<sup>-1</sup> and the band was composed by several overlapping peaks. CO stretching mode signals were deconvoluted on the basis of a Gaussian model

Table 1. IR band assignments for Au/TiO <sub>2</sub> DP-UC samples.		
Species	$\nu_{\text{CO}}$ [cm <sup>-1</sup> ]	Ref.
Linearly adsorbed CO on Au <sup>0</sup>	2106	[32,44,48–50]
Linearly adsorbed CO on Au <sup>δ-</sup>	2072	[11,51–56]
Multisite and bridged CO on Au <sup>δ-</sup>	2054–2043–2013	[7,27,43,58]

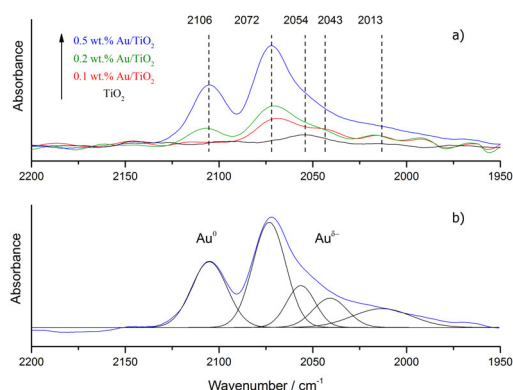


**Figure 1.** DRIFTS spectra of CO adsorbed at 298 K on 0.1, 0.2, and 0.5 wt% Au/TiO<sub>2</sub> (a) and detailed deconvolution for 0.5 wt% Au/TiO<sub>2</sub> (b).

using the Origin software. Results of this procedure are shown in Figure 1b. The presence of other bands at frequencies lower than 2100 cm<sup>-1</sup> is not common like the linear adsorption of CO at 2100–2120 cm<sup>-1</sup>. Some publications reported the formation of these bands at lower frequencies for catalysts where Au was strongly reduced.<sup>[11,51–57]</sup> Their origin is attributed to the linear and multisite adsorption (probably bridged-bond configuration) of CO on negatively charged gold (Au<sup>δ-</sup> sites). A detailed approach is presented by Sterrer et al.,<sup>[58]</sup> for an Au-MgO film, where the position of the bands was directly correlated to the charge of the site with a strong redshift owing to the  $\pi$ -back-donation of the negatively charged metal to the CO antibonding orbital. Also, the degree of coordination to the site, which is tightly correlated with the shape and size of the nanoparticle, has an influence. Boronat et al., confirmed this phenomenon, underlining that the shift in the  $\nu_{\text{CO}}$  frequency depends not only on the charge of the particle, but also on the degree of coordination of gold atoms and the capability of CO to modify the particle shape.<sup>[59]</sup> The shift of the bands due to the adsorption conformation of CO on the metal particles is well known also for other elements, especially for Pt-based catalysts.<sup>[60,61]</sup> In a recent work, Rogers et al. prepared several Au/TiO<sub>2</sub> catalysts by using a standard sol-immobilization technique with NaBH<sub>4</sub> as the final reductant. No peaks relative to Au<sup>+</sup> cations were detected, whereas bands at 2115 cm<sup>-1</sup> and 2040 cm<sup>-1</sup> were attributed to metallic and partially negatively charged gold, respectively.<sup>[62]</sup>

Summarizing, it can be concluded that a lower frequency implies: (i) lower coordination to the metallic site, and (ii) smaller size of the gold particles. This is the explanation of the CO stretching bands observed in our Au/TiO<sub>2</sub> DP-UC catalysts and allows us to explain the observed overlapping peaks. In particular, the peak at 2072 cm<sup>-1</sup> can be attributed to a linear adsorption of CO on partially negative gold sites and peaks at lower frequencies (2054, 2043, 2013 cm<sup>-1</sup> for the sample with the highest metal loading) to multisite adsorption of CO in different bridged configurations, depending on the degree of back-donation of Au to CO.<sup>[7,27,43,58]</sup> The absence of carbonyl bands relative to oxidized gold Au<sup>n+</sup> implies that Au was entirely reduced to zerovalent species as expected by using excess of NaBH<sub>4</sub><sup>[53,63,64]</sup> and is in agreement with the XPS data.

The nature of the negative charge on gold is closely related to the support,<sup>[12]</sup> in particular regarding the charge transfer between gold particles and  $M^{3+}$  cations of the support lattice.<sup>[65,66]</sup>

To further elucidate the nature of the IR bands, DRIFTS spectra after various exposure times to CO were recorded (Figure 2a). In clear accordance with Chakarova et al.<sup>[29]</sup> for Au/SiO<sub>2</sub> catalysts and Bollinger et al.,<sup>[67]</sup> the increase in the exposure time involves a gradual reduction of Au<sup>0</sup> to Au<sup>δ-</sup> because of

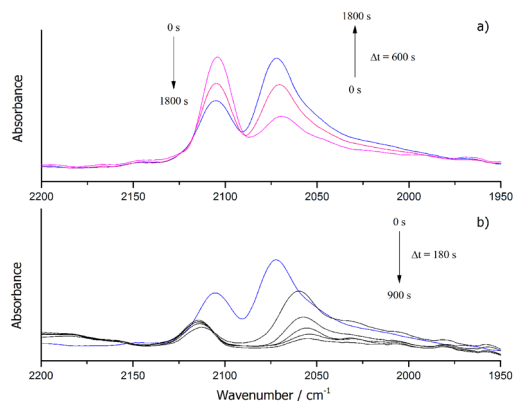


**Figure 2.** DRIFTS spectra of 0.5 wt% Au/TiO<sub>2</sub> at different CO exposure times (a) and during the evacuation after saturation (b).

the greater stability of the latter species, which is directly correlated with the greater  $\pi$ -back-donation.<sup>[68]</sup> Similar behavior was reported for other supported gold catalysts, including Au/MgO<sup>[27,58]</sup> and Au/CeO<sub>2</sub>.<sup>[54]</sup> This effect allows us to understand the absence of linear CO adsorption on Au<sup>0</sup>, which probably derives from complete reduction to the partially negative analog. These results underline the importance of reporting the interaction time between the probe molecule and the substrates during this powerful common analysis, because CO electronically modifies the catalyst surface.

The CO desorption analysis (Figure 2b) showed, as expected, a progressive redshift of the 2072 cm<sup>-1</sup> band owing to the higher stability of the different carbonyls formed on Au. However, a low intensity band at 2114 cm<sup>-1</sup>, blueshifted during the desorption with respect to the initial 2106 cm<sup>-1</sup> owing to the surface coverage effect,<sup>[69]</sup> still remained after 900 s. The very small amount of low coverage CO bound to Au<sup>0</sup> was probably related to the residual CO in the gas feed, which was very hard to remove totally.

For bare TiO<sub>2</sub>, only one very low intensity band appeared at 2054 cm<sup>-1</sup>. This data ruled out any possibility to attribute a strong contribution of CO-Ti<sup>n+</sup> interactions for the metal loaded samples, because only low-temperature CO adsorption can allow us to monitor this weak interaction.<sup>[70]</sup> This explanation was in accordance with the spectroscopic IR investigations carried out by our group at lower temperature on Ni and Cu supported on TiO<sub>2</sub><sup>[71,72]</sup> and other groups with Au/TiO<sub>2</sub> samples.<sup>[7,40,41,52]</sup>

A direct proportional correlation between the area of the IR CO stretching band and metal loading was obtained as pre-

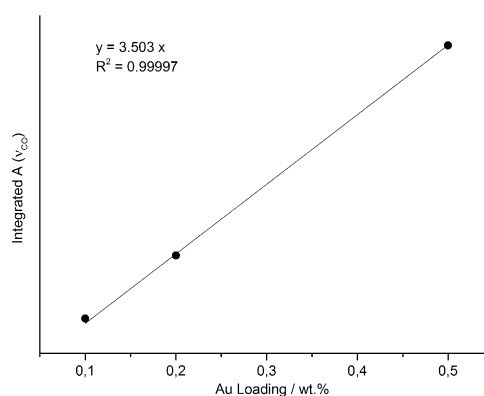


**Figure 3.** Integrated area of the CO stretching bands in the DRIFTS spectra (2106–2013 cm<sup>-1</sup>) versus Au loading (wt%).

sented in Figure 3. In general, the interpretation of intensities and the area of the DRIFT signals are difficult due to the several variables involved in the analysis, such as cell geometry, sample loading procedure, and deposition method used.<sup>[11]</sup> However, a strong direct correlation was observed here. This means that the variation of Au dispersion among the catalysts was too small to see variation in the position and intensity of the bands IR spectra. Moreover, it also means that the type of metal sites formed can be considered as being similar because otherwise different CO adsorption, which can be linear or multistate, would not lead to such a direct correlation.

The attribution of the low frequency broad band to the multistate adsorption with different configurations on partially negatively charged gold sites with a slightly different degree of back-donation between Au and CO is clearly in accordance with DFT calculations carried out by Rogers et al. for Au/TiO<sub>2</sub> DRIFT analysis.<sup>[62]</sup> The presence of these gold species could be related to the last chemical reduction step used during the synthesis. Indeed, recently Rojas et al. synthesized several Au/TiO<sub>2</sub> samples by a DP method using urea but with a final high-temperature reduction step in H<sub>2</sub> and they did not observe the negatively charged gold species by CO IR spectroscopy.<sup>[74]</sup> Conversely, Sandoval and co-workers obtained CO stretching bands at lower frequencies, although they used the DP-urea method with a final H<sub>2</sub> step so this point still remains unclear.<sup>[75]</sup> The assignment of the carbonyl stretching bands needed further investigation and, thus, we used a combination of complementary techniques to shed light on the metal nanoparticle properties.

### Morphologic and electronic characterization

The gold particle size distribution was determined by HRTEM and STEM. The representative images and respective histograms are shown in Figure 4 and these confirmed that the DP-UC method led to very narrow gold particle size distribution fitted by a log-normal curve. The mean diameter of Au particle size and relative standard deviation are presented in Table 2. These results allow us to better explain the attribution of the broad band at low frequency observed in the DRIFTS spectra.

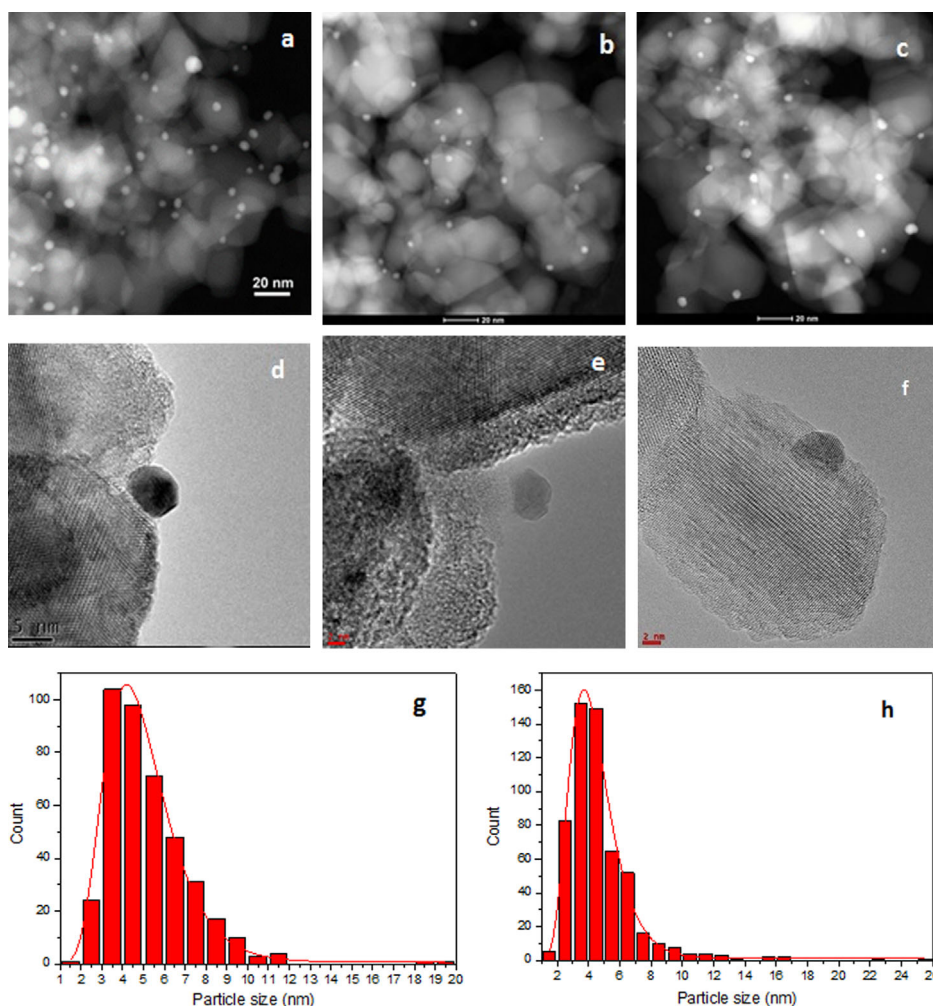


**Figure 4.** Representative STEM (a, b, c), HRTEM (d, e, f), and particle size distribution (g, h) images of a, d) 0.1 wt %, b, e, g) 0.2 wt %, and c, f, h) 0.5 wt % Au/TiO<sub>2</sub>. For STEM, scale bar = 20 nm. For HRTEM, scale bar = 5 nm for picture (d), scale bar = 2 nm for pictures (e) and (f).

**Table 2.** Statistical median of particle size analysis, specific surface area (SSA), XPS Au/Ti ratio and binding energy of Au4f<sub>7/2</sub> region data for gold-based catalysts.

Sample	Statistical median [nm]	Standard deviation [nm]	SSA [m <sup>2</sup> g <sup>-1</sup> ]	Au/Ti [mol/mol]	Au4f <sub>7/2</sub> BE [eV]	Au4f <sub>7/2</sub> BE after CO oxidation [eV]
0.1 wt % Au/TiO <sub>2</sub>	3.7	0.9	52	0.00226	83.6	83.6
0.2 wt % Au/TiO <sub>2</sub>	4.0	1.0	55	0.00260	83.6	83.7
0.5 wt % Au/TiO <sub>2</sub>	4.6	1.6	50	0.00482	83.6	83.6

Indeed, the broadening could be due to a multisite adsorption with different configurations or to bridged CO on differently sized gold nanoparticles. The combination of these techniques confirms the former hypothesis.

To elucidate the nature of the gold species, XPS was employed. The Au4f XPS spectra of Au/TiO<sub>2</sub> samples are shown in Figure 5 where the characteristic doublet of the two spin-orbit components are visible (Au4f<sub>7/2</sub> and Au4f<sub>5/2</sub> transitions). The oxidation state of Au at the surface of the catalyst was evaluated by analyzing the values of binding energy (BE) of the Au4f<sub>7/2</sub> peak. The BE of 83.6 ± 0.2 eV corroborates the results obtained by FTIR and TEM in that Au is in the metallic state

(Au<sup>0</sup>) and well dispersed without Au<sup>n+</sup> species (BE = 85.5 and 86.3 eV).<sup>[37,76–78]</sup> The slight decrease to a lower BE than the typical values obtained for metallic gold could be attributable to the different charging of the metal particles or to the particle size effect.<sup>[79]</sup> HRTEM and STEM analysis ruled out any possible size effects (a negative shift should be related to much bigger particle size), therefore, in accordance with the DRIFTS results, lower values of BE were attributed to the contribution of gold with partially negative charge.<sup>[80]</sup> The contribution of Au<sup>δ-</sup> was smaller with respect DRIFTS analysis because XPS was carried out without CO. As a final remark, the increase in the intensity in the XPS data fits well with the increase in metal loading. For

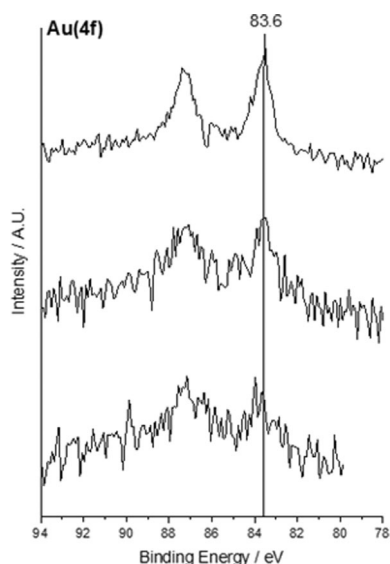


**Figure 5.** XPS spectra of the Au 4f region for 0.1, 0.2, and 0.5 wt% Au/TiO<sub>2</sub> samples (from the bottom to the top, respectively).

completeness, Ti2p spectra are reported in the Supporting Information (Figure S1) to confirm the state of TiO<sub>2</sub>. The same values of binding energies were detected for every sample (458.2 eV), irrespective of Au loading.

### Structure–activity correlation for CO oxidation

To get a closer insight into the relationship between the results obtained, CO oxidation activity tests were performed. For this process, finely dispersed nanoparticles are very important because bulk gold proved chemically inactive.<sup>[19,59]</sup> Moreover, understanding the active electronic state is fundamental to explain the mechanisms involved in the oxidative process.<sup>[81]</sup> Tests were carried out at room temperature without the addition of water to rule out the influence of its variation.<sup>[82]</sup> Sample 0.5 wt% Au/TiO<sub>2</sub> showed at room temperature a TOF-Ns =  $(6.1 \pm 0.3) \times 10^{-3} \text{ h}^{-1}$  and steady-state conditions were achieved after 20 min. A prolonged activity test under the reaction conditions was carried out for more than 6 h without any decrease in conversion, as shown in Figure 6. This fact confirmed the stability under the operating conditions adopted, with no appreciable deactivation.

The effect of temperature was studied for every catalyst and the relative Arrhenius plots are reported in Figure 7. The apparent activation energy of the CO oxidation reaction in the 298–373 K range was estimated from the slope of the logarithm of the intrinsic kinetic rate ( $\text{mols}^{-1} \text{g}_{\text{cat}}^{-1}$ ) versus  $T^{-1} \times 10^3 \text{ (K}^{-1}\text{)}$  plot. Similar values of activation energy were obtained for 0.1 wt% Au and 0.2 wt% Au, whilst a significantly lower value was calculated for the highest metal loaded sample. These values fall in the typical range reported in the literature for CO oxidation under dry conditions<sup>[67,83]</sup> (Table 3) and for Au/TiO<sub>2</sub> prepared by the DP-urea method,<sup>[75]</sup> although in general a strict comparison should consider that the activation energy is directly correlated with the particle size, surface area, CO

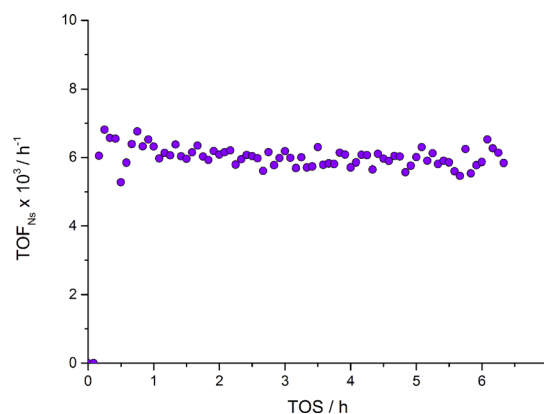


**Figure 6.** Time-on-stream (TOS) data expressed in TOF-Ns ( $\text{h}^{-1}$ ) for 0.5 wt% Au/TiO<sub>2</sub> ( $T = 298 \text{ K}$ ,  $\text{GHSV} = 4094 \text{ h}^{-1}$ , 5000 ppm CO in synthetic air).

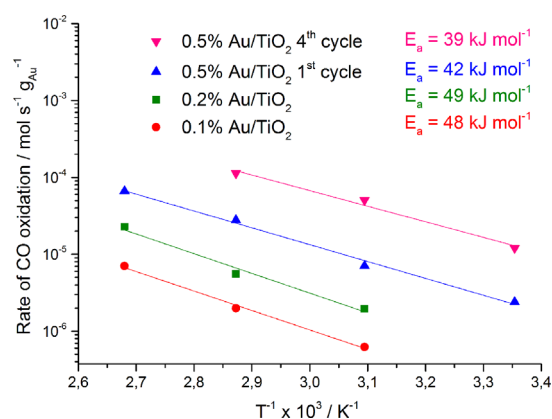


**Figure 7.** Arrhenius plots and relative apparent activation energies for the CO oxidation process for 0.1 wt% (orange), 0.2 wt% (green), 0.5% (blue), and 0.5 wt% Au/TiO<sub>2</sub> after the fourth cycle (pink).

**Table 3.** Comparison of Au/TiO<sub>2</sub> catalysts synthesized and tested for CO oxidation processes.

Au loading [wt%]	Au particle size [nm]	Preparation method	Apparent $E_a$ [ $\text{kJ mol}^{-1}$ ]	Refs.
0.1–0.5	3.7–4.6	DP-UC	39–48	This work
0.1–1.0	2–10	DP-NaOH	35–39	[92]
0.1	–	PAMAM	82	[93]
4.0	3.2	DP-U	35	[75]

concentration, and residence time. We achieved relatively low activation energy with lower Au loading and much more uniform Au particle size with respect to other literature reports.

To ensure a kinetically controlled regime with the operating conditions adopted, several tests at room temperature in which the space velocity was varied in the range 4000–16000  $\text{h}^{-1}$  were carried out (Figure 8). The linear increase in the TOF with increasing contact time (Figure 9) was clear proof that under the given reaction conditions diffusional transport effects were negligible. The results demonstrated the activity of metallic and partially negative Au also at such very low

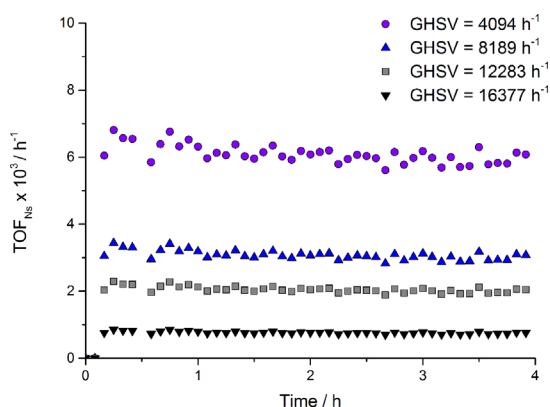


**Figure 8.** Influence of the space velocity in the range 4094–16377 h<sup>-1</sup> (2.44–0.61 h in terms of contact time) for 0.5 wt% Au/TiO<sub>2</sub> (*T* = 298 K, 5000 ppm CO in synthetic air).

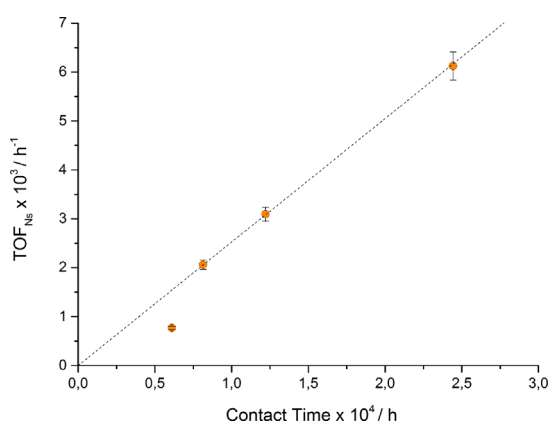


**Figure 9.** Linear plot of TOF versus contact time in the range 2.44–0.61 h (4094–16377 h<sup>-1</sup> in term of gas hourly space velocity) for 0.5 wt% Au/TiO<sub>2</sub> (*T* = 298 K, 5000 ppm CO in synthetic air).

loading. An important contribution was given by the presence of low coordinated Au sites in accordance with DFT calculations.<sup>[84]</sup>

To better understand the role of metal loading at this very low concentration for samples prepared by this new modified in situ deposition method (DP-UC), the Au% surface obtained from the Au/Ti ratio from the XPS atomic composition data and the Au% bulk values were plotted versus the CO oxidation rate at 323 K (Figure 10). The trend observed confirms the direct relationship between the catalytic activity, the dispersion, and the number of active sites exposed on the oxidic surface. This fact also means that all the metal deposited by this modified DP method remains on surface without penetrating inside pores or into the material bulk.

The role of the support in the CO oxidation reaction is fundamental.<sup>[12]</sup> In this specific case, the primary function is the stabilization of Au nanoparticles, which, otherwise, would coalesce irreversibly. Furthermore, as confirmed by DRIFTS analysis, the CO–Ti<sup>n+</sup> interactions are very weak, and indeed they do not directly influence the process. However, the electronic density and distribution of the AuNPs are strongly perturbed by interactions with the support, with related consequences

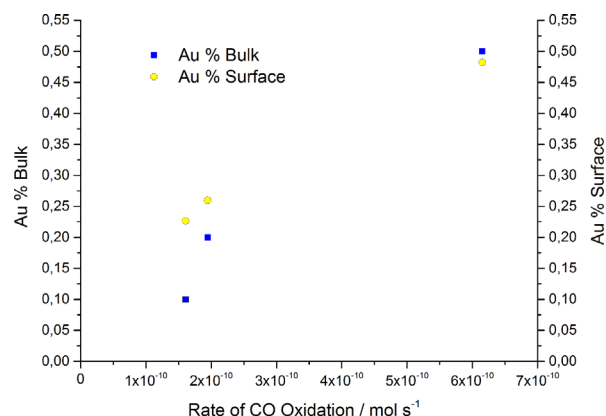


**Figure 10.** Au% surface and Au% bulk plotted versus rate of CO oxidation.

on the catalytic activity, especially in the case of oxides. In addition, surface hydroxyls promote the charge transfer between CO and AuNPs, changing the activation energy of the process.<sup>[82]</sup> The state of TiO<sub>2</sub> in the samples was confirmed by XPS analysis and did not vary appreciably with Au loading (Figure S1).

For the sample with the best activity, that is, the one with 0.5 wt% metal loading, repeated cycles were performed at different temperatures by using a GHSV equal to 8200 h<sup>-1</sup> (Figure 11). The results for subsequent cycles were substantially different, showing an increase in catalytic activity. Several factors could influence this phenomenon: a) variation of particle size; b) variation of the gold oxidation state; c) alteration of the water content; d) decrease of the carbon layer formed during the synthesis from urea decomposition.

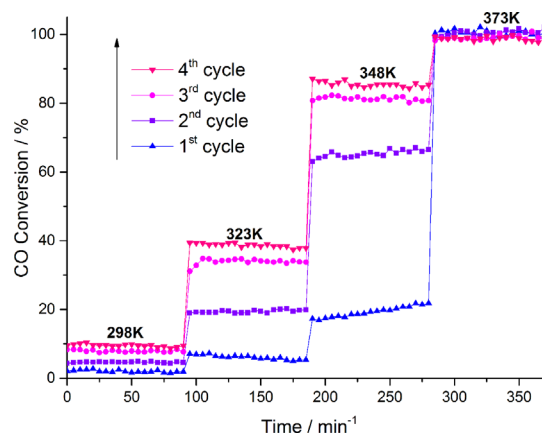


**Figure 11.** Repeated cycles of activity tests at different temperatures for 0.5 wt% Au/TiO<sub>2</sub>.

The low operating temperature ( $\geq 373$  K) ruled out any sintering phenomena, and the increase in activity from the first to the last cycle further confirmed that no increase in particle size occurred. The comparison of the XPS data for the Au4f<sub>7/2</sub> peak of the fresh and used samples (Table 2) indicated that no change of oxidation state occurred during the reaction and the BE typical of zerovalent gold was detected for the spent

samples. Therefore, the variation of catalytic activity for subsequent runs cannot be attributed to the variation of the metal oxidation state, because the BE of the Au after the first run showed approximately the same value as that after the fourth run. No change in water content was detected during the chromatographic analysis. Thus, subsequent investigations aimed at evaluating the presence of organic compounds on the surface, as is common when preparing metal nanoparticles by using organic agents.

Lari et al. reported the influence of thermal treatment for 1 wt% Au/TiO<sub>2</sub> samples prepared by sol-immobilization with stabilizing ligands such as PVP (polyvinylpyrrolidone) and PVA (polyvinyl alcohol) and naked supported gold nanoparticles prepared by DP.<sup>[69]</sup> They observed higher activity for the DP catalyst before any heat treatment because a lower amount of carbon was present on the surface. Comotti et al. drew the same conclusions when using a protecting agent and studying with repeated cycles to test the inhibitory effect of the organic protector on the surface for CO oxidation.<sup>[69]</sup> However, in those papers, the DP method for the deposition of the gold did not make use of urea. To explain this last hypothesis, the fresh catalyst was investigated by using DRIFTS without any probe molecule. In the beginning, a comparison between IR spectra at room temperature for Au/TiO<sub>2</sub> samples and bare P25-TiO<sub>2</sub> was done but without the detection of any significant bands from their subtraction. However, differences between the bare P25 and samples with Au appeared during IR analyses at different temperatures. The spectra of 0.5 wt% Au/TiO<sub>2</sub> were collected in the temperature range 373–420 K, and by investigating different exposure times at 420 K (30, 60, 90, 150 min). Spectra subtracted from the same analysis at room temperature are shown in Figure 12. The same procedure was carried out for the bare P25, but only with the gold catalyst did several bands appear in the region between 1000 and 2000 cm<sup>-1</sup>. In particular, strong signals at 1441 and 1317 cm<sup>-1</sup> appeared, with shoulder and lower peaks at 1583, 1486, 1277 cm<sup>-1</sup>, without any band at higher wavenumbers. Unfortunately, broad desorption of physisorbed water did not allow peaks around

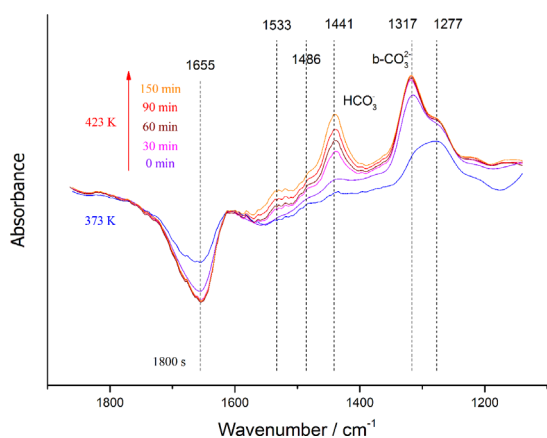


**Figure 12.** DRIFTS spectra of 0.5 wt% Au/TiO<sub>2</sub> under N<sub>2</sub> flow at different temperatures (373 and 423 K) and exposure times at 423 K (0, 30, 60, 90, and 150 min) subtracted from the spectrum collected at 298 K.

1650 cm<sup>-1</sup> to be revealed, and its elimination was impossible because any pre-treatment was done to maintain the same initial conditions adopted before the CO oxidation test. These bands belong to the carbonate region and can be assigned to N compounds or carbonate species formed during the decomposition of urea. Larrubia et al. in a adsorption/decomposition study of several N compounds including urea on iron–titania catalysts, obtained several strong bands attributed to the NH–C=O stretching mode near 1565, 1490 cm<sup>-1</sup>, and in the region below 1300 cm<sup>-1</sup>.<sup>[85]</sup> Fang et al. reported a similar attribution for the urea thermolysis for the urea-SCR process; in particular, bands at 1500 cm<sup>-1</sup> attributed to the imine group and at 1100 cm<sup>-1</sup> attributed to C–O linkages derive from the keto-enol configuration exchange.<sup>[86]</sup> Recently, Bernhard et al. confirmed the presence of these lower frequency bands and they attributed the band around 1560 cm<sup>-1</sup> to the asymmetric Ti–OCN–Ti stretching mode of adsorbed urea on titania.<sup>[87]</sup> However, in contrast with these results, no peaks at higher wavenumbers were detected in our analysis and, moreover, no N 1s peak was revealed in the XPS data in the BE region around 400 eV. This can be explained by the removal of carbamate and NH<sub>3</sub> in the washing procedure and heat treatments performed during the synthesis. Therefore, the attribution was carried out by considering the carbonate formed during the urea decomposition step, because formed CO<sub>2</sub> can react in small part with lattice oxygen on the gold–support interface.<sup>[52]</sup> The strong peak at 1317 cm<sup>-1</sup> was assigned to the bidentate carbonate (b-CO<sub>3</sub><sup>2-</sup>) on titania surface,<sup>[88]</sup> whereas the peak at 1441 cm<sup>-1</sup> was assigned to the bicarbonate (HCO<sub>3</sub><sup>-</sup>) species. The other peaks at 1533, 1486, and 1277 cm<sup>-1</sup> can be attributed to weak signals relative to the presence of carbonate.<sup>[89]</sup>

CO adsorption before and after thermal treatment did not show any shift of the CO stretching bands, and this means that: i) the carbon layer present on the surface is very thin because it did not prevent the adsorption of CO on gold nanoparticles such as in the case of syntheses that use protecting agents;<sup>[69,90]</sup> ii) the presence of this thin organic layer did not influence the gold dispersion or its electronic state. The attribution of the bands for the present samples was in accordance with the interpretation summarized above and it was confirmed by further characterization through XPS, which is a powerful tool to obtain quantitative and qualitative information on carbon amount over the surface of a catalyst.<sup>[33,91]</sup> A decrease in the organic content over the surface of the catalysts after the reaction was indeed confirmed, as a considerable loss of carbon was detected and monitored by the decreasing intensity of the C 1s peak (from 23.5 to 19.0 wt%).

## Conclusions

Supported Au nanoparticles on TiO<sub>2</sub> were synthesized by using a modified DP method combining urea as base and NaBH<sub>4</sub> for the chemical reduction step (DP-UC method). This technique allowed us to obtain highly dispersed nanoparticles at very low metal loading (0.1–0.5 wt%). An in depth characterization was carried out by means of DRIFT spectroscopy with CO as a probe. The formation of Au metallic nanoparticles with a con-

tribution of partially negatively charged Au was obtained. CO oxidation kinetic studies were carried out to correlate the physicochemical features of the prepared AuNPs with the catalytic activity. The explanation of the activity enhancement after subsequent runs was attributed to the release of a very thin carbon layer initially present on the catalyst surface. Characterization of fresh and spent samples allowed us to confirm and study the presence of these C compounds formed from urea decomposition during the synthesis, which in small part block some of the active sites of the catalyst. These results not only deepen the understanding of a modified gold deposition strategy, but also demonstrate a good activity for CO oxidation at lower loadings and without thermal treatment for the final reduction step of the synthesized Au nanoparticles.

## Acknowledgements

We would like to acknowledge the Erasmus Placement program for the scholarship attributed to Dr. M. Compagnoni supporting the internship at the Cardiff Catalysis Institute (Cardiff University).

**Keywords:** CO oxidation · deposition/precipitation method · DRIFTS · gold catalysis

- [1] F. Zaera, *Chem. Soc. Rev.* **2014**, *43*, 7624–7663.
- [2] C. Lamberti, A. Zecchina, E. Groppo, S. Bordiga, *Chem. Soc. Rev.* **2010**, *39*, 4951–5001.
- [3] K. Hadjiivanov, D. Klissurski, G. Ramis, G. Busca, *Appl. Catal. B* **1996**, *7*, 251–267.
- [4] W. Zhou, Y. Zhang, M. Abe, K. Uosaki, M. Osawa, Y. Sasaki, S. Ye, *Langmuir* **2008**, *24*, 8027–8035.
- [5] G. Busca, *Catal. Today* **1998**, *41*, 191–206.
- [6] I. Rossetti, G. F. Mancini, P. Ghigna, M. Scavini, M. Piumetti, B. Bonelli, F. Cavani, A. Comite, *J. Phys. Chem. C* **2012**, *116*, 22386–22398.
- [7] K. I. Hadjiivanov, G. N. Vayssilov, *Adv. Catal.* **2002**, *47*, 307–511.
- [8] G. Blyholder, *J. Phys. Chem.* **1975**, *79*, 756–761.
- [9] S. Zou, R. Go, M. J. Weaver, *Langmuir* **1997**, *13*, 6713–6721.
- [10] C. Liu, M. Virginie, A. Griboval-Constant, A. Khodakov, *Appl. Catal. A* **2015**, *504*, 565–575.
- [11] M. A. Debeila, N. J. Coville, M. S. Scurrell, G. R. Hearne, *Catal. Today* **2002**, *72*, 79–87.
- [12] B. K. Min, C. M. Friend, *Chem. Rev.* **2007**, *107*, 2709–2724.
- [13] A. S. K. Hashmi, G. J. Hutchings, *Angew. Chem. Int. Ed.* **2006**, *45*, 7896–7936; *Angew. Chem.* **2006**, *118*, 8064–8105.
- [14] N. Dimitratos, J. A. Lopez-Sanchez, G. J. Hutchings, *Chem. Sci.* **2012**, *3*, 20–44.
- [15] N. Lopez, T. V. W. Janssens, B. S. Clausen, Y. Xu, M. Mavrikakis, T. Bligaard, *J. Catal.* **2004**, *223*, 232–235.
- [16] G. J. Hutchings, *Top. Catal.* **2014**, *57*, 1265–1271.
- [17] G. Li, L. Li, D. Jiang, *J. Phys. Chem. C* **2015**, *119*, 12502–12507.
- [18] M. Du, D. Sun, H. Yang, J. Huang, X. Jing, T. Odoom-wubah, H. Wang, L. Jia, Q. Li, *J. Phys. Chem. C* **2014**, *118*, 19150–19157.
- [19] M. Haruta, *Chem. Rec.* **2003**, *3*, 75–87.
- [20] S. Lin, X. Ye, R. S. Johnson, H. Guo, *J. Phys. Chem. C* **2013**, *117*, 17319–17326.
- [21] I. Rossetti, C. Biffi, G. F. Tantardini, M. Raimondi, E. Vitto, D. Alberti, *Int. J. Hydrogen Energy* **2012**, *37*, 8499–8504.
- [22] I. Rossetti, M. Compagnoni, M. Torli, *Chem. Eng. J.* **2015**, *281*, 1036–1044.
- [23] E. D. Park, J. S. Lee, *J. Catal.* **1999**, *186*, 1–11.
- [24] M. Daté, M. Haruta, *J. Catal.* **2001**, *201*, 221–224.
- [25] F. Boccuzzi, A. Chiorino, *J. Phys. Chem. B* **2000**, *104*, 5414–5416.
- [26] D. Chen, K. O. Christensen, E. Ochoa-Fernández, Z. Yu, B. Tørdal, N. Latorre, A. Monzón, A. Holmen, *J. Catal.* **2005**, *229*, 82–96.
- [27] B. Yoon, H. Häkkinen, U. Landman, A. S. Wörz, J.-M. Antonietti, S. Abbet, K. Judai, U. Heiz, *Science* **2005**, *307*, 403–407.
- [28] W. T. Wallace, R. L. Whetten, *J. Am. Chem. Soc.* **2002**, *124*, 7499–7505.
- [29] K. Chakarova, M. Mihaylov, S. Ivanova, M. A. Centeno, K. Hadjiivanov, *J. Phys. Chem. C* **2011**, *115*, 21273–21282.
- [30] R. Zanella, L. Delannoy, C. Louis, *Appl. Catal. A* **2005**, *291*, 62–72.
- [31] W. C. Li, M. Comotti, F. Schüth, *J. Catal.* **2006**, *237*, 190–196.
- [32] T. Venkov, K. Fajerberg, L. Delannoy, H. Klimev, K. Hadjiivanov, C. Louis, *Appl. Catal. A* **2006**, *301*, 106–114.
- [33] N. Dimitratos, J. A. Lopez-Sanchez, D. Morgan, A. Carley, L. Prati, G. J. Hutchings, *Catal. Today* **2007**, *122*, 317–324.
- [34] L. Prati, A. Villa, *Catalysts* **2011**, *2*, 24–37.
- [35] S. Chen, B. Zhang, D. Su, W. Huang, *ChemCatChem* **2015**, *7*, 3290–3298.
- [36] K. C. Petalidou, S. Boghosian, A. M. Efstathiou, *Catal. Today* **2015**, *242*, 153–167.
- [37] N. Dimitratos, A. Villa, C. L. Bianchi, L. Prati, M. Makkee, *Appl. Catal. A* **2006**, *311*, 185–192.
- [38] H. Huang, X. Ye, H. Huang, L. Zhang, D. Y. C. Leung, *Chem. Eng. J.* **2013**, *230*, 73–79.
- [39] F. E. López-Suárez, A. Bueno-López, K. I. B. Eguiluz, G. R. Salazar-Banda, *J. Power Sources* **2014**, *268*, 225–232.
- [40] A. Kumar, V. Pavan, V. P. Kumar, B. P. Kumar, V. Vishwanathan, K. V. R. Chary, *Catal. Lett.* **2014**, *144*, 1450–1459.
- [41] F. Boccuzzi, A. Chiorino, *J. Phys. Chem.* **1996**, *100*, 3617–3624.
- [42] D. A. Panayotov, S. P. Burrows, J. T. Yates, J. R. Morris, *J. Phys. Chem. C* **2011**, *115*, 22400–22408.
- [43] J. Wang, V. F. Kispersky, W. Nicholas Delgass, F. H. Ribeiro, *J. Catal.* **2012**, *289*, 171–178.
- [44] F. Boccuzzi, A. Chiorino, M. Manzoli, P. Lu, T. Akita, S. Ichikawa, M. Haruta, *J. Catal.* **2001**, *202*, 256–267.
- [45] S. Oros-Ruiz, R. Zanella, R. López, A. Hernández-Gordillo, R. Gómez, *J. Hazard. Mater.* **2013**, *263*, 2–10.
- [46] K. Mori, T. Hara, T. Mizugaki, K. Ebitani, K. Kaneda, *J. Am. Chem. Soc.* **2004**, *126*, 10657–10666.
- [47] M. Comotti, C. Della Pina, R. Matarrese, M. Rossi, *Angew. Chem. Int. Ed.* **2004**, *43*, 5812–5815; *Angew. Chem.* **2004**, *116*, 5936–5939.
- [48] B. Schumacher, Y. Denkwitz, V. Plzak, M. Kinne, R. J. Behm, *J. Catal.* **2004**, *224*, 449–462.
- [49] M. Manzoli, A. Chiorino, F. Boccuzzi, *Surf. Sci.* **2003**, *532–535*, 377–382.
- [50] A. Villa, C. E. Chan-Thaw, G. M. Veith, K. L. More, D. Ferri, L. Prati, *ChemCatChem* **2011**, *3*, 1612–1618.
- [51] A. Villa, D. Ferri, S. Campisi, C. E. Chan-Thaw, Y. Lu, O. Kröcher, L. Prati, *ChemCatChem* **2015**, *7*, 2534–2541.
- [52] E. del Río, S. E. Collins, A. Aguirre, X. Chen, J. J. Delgado, J. J. Calvino, S. Bernal, *J. Catal.* **2014**, *316*, 210–218.
- [53] F. Boccuzzi, A. Chiorino, M. Manzoli, D. Andreeva, T. Tabakova, *J. Catal.* **1999**, *188*, 176–185.
- [54] T. Tabakova, F. Boccuzzi, M. Manzoli, D. Andreeva, *Appl. Catal. A* **2003**, *252*, 385–397.
- [55] J. D. Henao, T. Caputo, J. H. Yang, M. C. Kung, H. H. Kung, *J. Phys. Chem. B* **2006**, *110*, 8689–8700.
- [56] A. Villa, G. M. Veith, D. Ferri, A. Weidenkaff, K. A. Perry, S. Campisi, L. Prati, *Catal. Sci. Technol.* **2013**, *3*, 394–399.
- [57] A. M. Venezia, V. La Parola, G. Deganello, B. Pawelec, J. L. G. Fierro, *J. Catal.* **2003**, *215*, 317–325.
- [58] M. Sterrer, M. Yulikov, E. Fischbach, M. Heyde, H. P. Rust, G. Pacchioni, T. Risse, H. J. Freund, *Angew. Chem. Int. Ed.* **2006**, *45*, 2630–2632; *Angew. Chem.* **2006**, *118*, 2692–2695.
- [59] M. Boronat, P. Concepción, A. Corma, *J. Phys. Chem. C* **2009**, *113*, 16772–16784.
- [60] L.-C. de Ménorval, A. Chaqroune, B. Coq, F. Figueras, *J. Chem. Soc. Faraday Trans.* **1997**, *93*, 3715–3720.
- [61] T. Yajima, H. Uchida, M. Watanabe, *J. Phys. Chem. B* **2004**, *108*, 2654–2659.
- [62] S. M. Rogers, C. R. A. Catlow, C. E. Chan-Thaw, D. Gianolio, E. K. Gibson, A. L. Gould, N. Jian, A. J. Logsdail, R. E. Palmer, L. Prati, N. Dimitratos, A. Villa, P. P. Wells, *ACS Catal.* **2015**, *5*, 4377–4384.
- [63] L. Piccolo, H. Daly, A. Valcarcel, F. C. Meunier, *Appl. Catal. B* **2009**, *86*, 190–195.
- [64] S. Gaur, H. Wu, G. G. Stanley, K. More, C. S. S. R. Kumar, J. J. Spivey, *Catal. Today* **2013**, *208*, 72–81.

- [65] O. H. Laguna, A. Pérez, M. A. Centeno, J. A. Odriozola, *Appl. Catal. B* **2015**, *176–177*, 385–395.
- [66] M. Chen, Y. Cai, Z. Yan, D. W. Goodman, *J. Am. Chem. Soc.* **2006**, *128*, 6341–6346.
- [67] M. A. Bollinger, M. A. Vannice, *Appl. Catal. B* **1996**, *8*, 417–443.
- [68] M. Mihaylov, H. Knözinger, K. Hadjiivanov, B. C. Gates, *Chem. Ing. Tech.* **2007**, *79*, 795–806.
- [69] G. M. Lari, E. Nowicka, D. J. Morgan, S. A. Kondrat, G. J. Hutchings, *Phys. Chem. Chem. Phys.* **2015**, *17*, 23236–23244.
- [70] D. V. Kozlov, E. A. Paukshtis, E. N. Savinov, *Appl. Catal. B* **2000**, *24*, L7–L12.
- [71] G. Ramis, I. Rossetti, E. Finocchio, M. Compagnoni, M. Signoretto, A. Michele, *Prog. Clean Energy* **2015**, *1*, 695–711.
- [72] E. Finocchio, I. Rossetti, G. Ramis, *Int. J. Hydrogen Energy* **2013**, *38*, 3213–3225.
- [73] P. Konova, A. Naydenov, C. Venkov, D. Mehandjiev, D. Andreeva, T. Tabakova, *J. Mol. Catal. A* **2004**, *213*, 235–240.
- [74] H. a. Rojas, J. J. Martínez, G. Díaz, A. Gómez-Cortés, *Appl. Catal. A* **2015**, *503*, 196–202.
- [75] A. Sandoval, C. Louis, R. Zanella, *Appl. Catal. B* **2013**, *140–141*, 363–377.
- [76] S. Arrii, F. Morfin, A. J. Renouprez, J. L. Rousset, *J. Am. Chem. Soc.* **2004**, *126*, 1199–1205.
- [77] S. Albonetti, T. Pasini, A. Lolli, M. Blosi, M. Piccinini, N. Dimitratos, J. A. Lopez-Sanchez, D. J. Morgan, A. F. Carley, G. J. Hutchings, F. Cavani, *Catal. Today* **2012**, *195*, 120–126.
- [78] J. M. López, R. Arenal, B. Puértolas, Á. Mayoral, S. H. Taylor, B. Solsona, T. García, *J. Catal.* **2014**, *317*, 167–175.
- [79] C. C. Chusuei, X. Lai, K. Luo, D. W. Goodman, *Top. Catal.* **2000**, *14*, 71–83.
- [80] A. Zwijnenburg, A. Goossens, W. G. Sloof, M. W. J. Craje, *J. Phys. Chem. B* **2002**, *106*, 9853–9862.
- [81] O. P. Tkachenko, A. A. Greish, A. V. Kucherov, K. C. Weston, A. M. Tsybullevski, L. M. Kustov, *Appl. Catal. B* **2015**, *179*, 521–529.
- [82] T. Fujitani, I. Nakamura, M. Haruta, *Catal. Lett.* **2014**, *144*, 1475–1486.
- [83] M. Haruta, M. Daté, *Appl. Catal. A* **2001**, *222*, 427–437.
- [84] I. N. Remediakis, N. Lopez, J. K. Nørskov, *Appl. Catal. A* **2005**, *291*, 13–20.
- [85] M. A. Larrubia, G. Ramis, G. Busca, *Appl. Catal. B* **2000**, *27*, L145–L151.
- [86] H. L. Fang, H. F. M. Da Costa, *Appl. Catal. B* **2003**, *46*, 17–34.
- [87] A. M. Bernhard, D. Peitz, M. Elsener, O. Kröcher, *Top. Catal.* **2013**, *56*, 130–133.
- [88] W. Su, J. Zhang, Z. Feng, T. Chen, P. Ying, C. Li, *J. Phys. Chem. C* **2008**, *112*, 7710–7716.
- [89] Z. Bacsik, N. Ahlsten, A. Ziadi, G. Zhao, A. E. Garcia-Bennett, B. Martín-Matute, N. Hedin, *Langmuir* **2011**, *27*, 11118–11128.
- [90] F. Zaera, *ChemCatChem* **2012**, *4*, 1525–1533.
- [91] T. Böcking, K. a. Kilian, T. Hanley, S. Ilyas, K. Gaus, M. Gal, J. J. Gooding, *Langmuir* **2005**, *21*, 10522–10529.
- [92] F. Moreau, G. Bond, A. Taylor, *J. Catal.* **2005**, *231*, 105–114.
- [93] B. J. Auten, H. Lang, B. D. Chandler, *Appl. Catal. B* **2008**, *81*, 225–235.

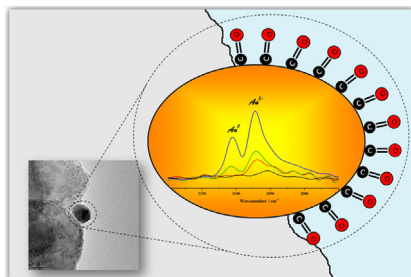
Received: January 21, 2016

Revised: February 26, 2016

Published online on ■ ■ ■, 0000

## FULL PAPERS

**Gold nanoparticles on titania:** Diffuse reflectance infrared Fourier transform spectroscopy (DRIFTS), coupled with CO adsorption, was used to investigate a modified deposition/precipitation method (DP-UC) for the preparation of supported gold nanoparticles with very low metal loading (0.1–0.5 wt%). This promising synthetic route involves the use of urea as basic agent and  $\text{NaBH}_4$  as chemical reductant in contrast to the traditional high-temperature reduction step.



*M. Compagnoni,\* S. A. Kondrat, C. E. Chan-Thaw, D. J. Morgan, D. Wang, L. Prati, A. Villa, N. Dimitratos, I. Rossetti\**



**Spectroscopic Investigation of Titania-Supported Gold Nanoparticles Prepared by a Modified Deposition/Precipitation Method for the Oxidation of CO**

